PGM1 Suppresses Colorectal Cancer Cell Migration And Invasion by Regulating PI3K/ AKT Pathway

Zhewen Zheng
  Wuhan University

Xue Zhang
  Capital Medical University

Jian Bai
  Peking University

Long Long
  Wuhan University

Di Liu
  Wuhan University

Yunfeng Zhou (✉ 2017103030046@whu.edu.cn)
  Wuhan University   https://orcid.org/0000-0003-4328-6646

Abstract

Background

Phosphoglucomutase 1(PGM1) is known for its involvement in cancer pathogenesis. However, its biological role in colorectal cancer (CRC) is unknown. Here, we studied the functions and mechanisms of PGM1 in CRC.

Methods

We verified PGM-1 as a DEG by a comprehensive strategy of the TCGA-COAD dataset mining and computational biology. Relative levels of PGM-1 in CRC tumors and adjoining peritumoral tissue were identified by qRT-PCR, WB, and IHC staining in a tissue microarray. PGM1 functions were analyzed using CCK8, EdU, colony formation, cell cycle, apoptosis, and Transwell migration and invasion assays. The influence of PGM1 was further investigated using tumor formation in vivo.

Results

PGM1 mRNA and protein were both reduced in CRC and the reduction was related to CRC pathology and overall survival. PGM1 knockdown stimulated both proliferation and colony formation, promoting cell cycle arrest and apoptosis while overexpression has opposite effects in CRC cells both *in vivo* and *in vitro*. Furthermore, we lined the actions of PGM1 to the PI3K/ AKT pathway.

Conclusion

We verified that PGM1 suppresses CRC through the PI3K/ AKT pathway. These results suggest the potential for targeting PGM1 in CRC therapies.

Background

Colorectal cancer (CRC) results in a high number of cancer-related deaths throughout the world [1]. In the USA, 147 950 new cases were reported in 2020 and around 53 200 deaths are reported annually [2]. Primary therapy options mainly depend on CRC staging. The five-year survival rate for early-stage disease is above 90% [1, 3]. Unfortunately, many patients already have advanced-stage disease at diagnosis [4]. There is, therefore, a need for identifying reliable biomarkers and cancer-related molecular mechanisms to assist with decisions regarding the patient's prognosis and suitable therapeutic strategies.

The microenvironment of a tumor plays a critical role in metastatic spread. Increased glycolytic activity is associated with increasing microenvironmental energy demands [5, 6] and tumors are characterized by a switch from oxidative phosphorylation to glycolysis as their main source of energy [7] with biosynthesis within the cell supplying the necessary components and imparting a selective advantage to the neoplastic cell [8]. Phosphoglucomutase (PGM) plays a key role in glucose metabolism [9], and the enzyme has been linked to cancer growth, metastasis, and invasion [10, 11]. Phosphoglucomutase 1

(PGM1) is encoded by the *PGM1* gene; *PGM1* deficiency is a recognized inherited metabolic disorder (CDG1T) that is linked to a variety of diseases and disorders, including liver disease, exercise intolerance, and dilated cardiomyopathy, a reflection of the key role played by the enzyme in glucose metabolism [12–14].PGM1 inhibits Hepatocellular Carcinoma (HCC) proliferation and growth by utilizing sufficient extracellular glucose to convert glycogen, while deletion of the gene inhibits glycogen synthesis and leads to glycolysis of more glucose, thus promoting tumor cell proliferation and growth [15]. However, PGM1 showed the opposite effect in lung cancer; researchers identified that *PGM1* upregulation decreased glycogen content, thereby reducing the rate of glycogen decomposition and glycogenesis, further depressing long-term repeated glucose consumption and inhibiting lung cancer cell proliferation [16]. Thus, *PGM1* plays a tumor-promoting or anti-tumor-promoting role in an environmentally-dependent way.

Here, we investigated the role of PGM1 and its regulation in CRC. We identified a new mechanism by which PGM1 suppresses CRC progression by regulating glucose translocation by the PI3K/ AKT pathway.

Materials And Methods

TCGA data sets

Differentially expressed genes were investigated using TCGA COAD (colorectal adenocarcinoma) and READ (rectal adenocarcinoma) data sets. The Ballgown R package in Bioconductor was used to analyze differential expression in RNA-seq data. Gene expression was compared between cancer and adjoining non-cancerous tissue. P-values and differences between the q-value and fold change were calculated using the following criteria for differential expression: P<0.01, q<0.05, and fold change >2. GEPIA (gepia.cancer-pku.cn) was used for normalization and log2-scaling.

Collection of clinical samples

This study was approved by the institutional review board of Wuhan University Zhongnan Hospital. Written informed consent was obtained from patients before sample collection.

Samples (tumor and adjoining normal tissue) were collected from 76 primary CRC patients admitted to Wuhan University Zhongnan Hospital between July 2019 and October 2020. Samples were frozen at −80°C until use. The patients' clinical information is provided in Table 1.

Immunohistochemistry and scoring

Immunohistochemical analysis (IHC) was done with a CRC tissue microarray (TMA) slide (Cat: HColA180Su10, Shanghai Outdo Biotech Co., Ltd., China). The TMA included CRC tissues from 100 surgically resected patients from April to November 2008. These patients were followed up until July 2015 (range 6.7-7.2 yr), had a mean age of 66.83 yr (range 45-91 yr), and included 58 men and 41 women. Table S1 shows the clinical data of these patients.   Sections (4μm thick) were cut and deparaffinized. Sections were microwaved for 5 min in citric acid (pH 6.0), and incubated with an anti-PGM1 antibody (#15161-1-AP, Proteintech, China,1:200, overnight, 4°C), and then incubated with

secondary antibody. The images were examined by two blinded pathologists and scored by multiplying the staining intensity (grades 0, 1, and 2 indicated negative, grade 3, weakly positive, grade 4, moderately positive, and grade 5, strongly positive) by the positive rate score (score 0 = 0%, 1 = 0-5%, 2 = 6-25%, 3 = 26-50%, 4 = 51-75%, and 5 = 76-100%).

Cell culture

Human CRC lines HT-29, LoVo, COLO205, SW620, and HCT116, together with the normal human colorectal cell line HCoEpic, were provided by the Institute of Biochemistry and Cell Biology of the Chinese Academy of Sciences (Shanghai, China). They were cultured in DMEM (Gibco, USA) with 10% fetal bovine serum (FBS, Gibco) at 37°C in a humidified chamber supplemented with 5% CO_2.

Western blotting

Western blotting was utilized to analyze PGM1 expression in tumor tissue and cultured cells. Lysis of tissues and cells was done with RIPA buffer (Beyotime, Beijing, China) with proteolytic inhibitors (Genebase, Shanghai, China) and protein concentrations measured with a Pierce BCA Protein Assay kit (Thermo Scientific, USA). Protein extracts (30 μg) were separated on 10–12% SDS-PAGE and blotted into transferred to polyvinylidene fluoride (PVDF) membranes (Millipore, Bedford, MA, USA). Blots were probed with primary antibodies including PGM1 (Abcam, #232959, 1:1000 dilution), PI3K (Abcam, #ab32089, 1:10000), p-PI3K (Abcam, #ab278545, 1:10000), AKT (Abcam, #ab8805, 1:10000), p-AKT (Abcam, #ab38449, 1:10000), Bcl-2 (Abcam, #ab182858, 1:10000), Bax (Abcam, #ab32503, 1:10000), p21 (Abcam, #ab109199, 1:10000), Cyclin D1 (Abcam, #ab40754, 1:10000), and GAPDH (CST, #3686, 1:1000) overnight at 4°C. Secondary antibodies were added room temperature, I h) followed by the ECL Western blotting Detection System (Amersham, Piscataway, NJ, USA). The loading control was GAPDH, and blots were run in triplicate. ImageJ software (was used for quantitation.

RT-PCR

Total RNA from the cells and tissues was isolated with TRIzol (Invitrogen, USA) and cDNA was obtained using a Bestar^{TM} qPCR RT kit (DBI Bioscience, #2220, Germany). The PGM1 primer was 5'-AGCATTCCGTATTTCCAGCAG-3' (forward) and 5'-GCCAGTTGGGGTCTCA TACAAA -3' (reverse). GAPDH primers were 5'-TGTTCGTCATGGGTGTGAAC-3' (forward) and 5'-ATGGCATGGACTGTGGTCAT-3' (reverse). PGM1 expression was measured by RT-PCR using Bestar^{TM} qPCR MasterMix (DBI Bioscience, #2043, Germany). The control was GAPDH, and the relative gene expression for determining mRNA levels was calculated by the $2^{-\Delta\Delta Ct}$ method [17].

Immunofluorescence (IF)

Immunofluorescence staining for cells was described before [18]. In brief, cells were fixed (4% paraformaldehyde, 15 min) in paraformaldehyde (4%) and permeabilized (0.1% Triton X-100, 10 min, 4°C). Primary antibodies were incubated overnight followed by secondary antibodies (60 min, room

temperature). DAPI was used for staining nuclei (5 min) and the sealed coverslips were evaluated using a laser scanning confocal microscope (Zeiss, Germany).

Immunohistochemistry (IHC), Ki 67, and H&E staining

For IHC, sections were deparaffinized and endogenous peroxide was inactivated. Sections were blocked and incubated with anti-PGM1 (Proteintech, #15161-1-AP, 1:200) or anti-Ki67 (Bbcam, #ab15580, 1:400) primary antibodies and secondary antibodies (Abcam, #ab205718, 1:4000). For H&E staining, sections of mouse xenograft tumors were deparaffinized and then rehydrated and stained with H&E (Sigma-Aldrich), before dehydration and sealing. Sections were assessed and photographed undera phase contrast microscopy (Leica, Cat. #DMI 1).

Transfection and plasmid construction

Cells (SW620 and HT-29) were transfected with plasmid or shRNA using Lipofectamine 2000, following instructions. The sense sequences of PGM1 short hairpin (sh)RNA -shPGM1 were: shRNA1, 5'-GGTCCTGCTCCAGA AG CAATA-3⬚, shRNA2, 5'-GGGATCATCACTGGTGGTTGG-3⬚, shRNA3, 5'-GCAGA TGGCAGCTGCCAATGG-3⬚. The sh-negative control (NC)-shCTRL was 5'-CAGT TGACGAGCAGTGC ATTT-3⬚. The PGM1 overexpression plasmid pcDNA4.0-PGM1 and empty plasmid pcDNA4.0 were obtained from Synbio Technologies Co. Ltd. (Suzhou, China). To construct stable PGM1 knockdown and overexpression cell lines, HT-29 and SW620 cells were treated with lentiviral control-shRNA (shCTRL), lentiviral-PGM1-shRNA-1 (shPGM1), lentiviral- pcDNA4.0-PGM1, lentiviral- pcDNA4.0 and selected using puromycin (5 μg/ml, Sigma).

Measurement of proliferation and colony formation

The CCK-8 assay (Dojindo Laboratories, Kumamoto, Japan) was used for evaluating proliferation. Triplicate samples of cells (2×10^3) were added to 96-well plates and the absorbance at 450 nm was determined each day for three days. For measuring colony formation, triplicate samples of treated cells (1.5×10^3) were grown for 14 days before washing twice (PBS), fixing (methanol, 10 min), and staining (0.1% crystal violet, 10 min).

EDU proliferation assay

Proliferation was also measured with an EdU kit (Ribobio, Guangzhou, China).The cells (10×10^5 per well) were inoculated in confocal plates in 50 μM EDU buffer and incubated (37°C, 2 h) before fixing (4% formaldehyde, 30 min) and permeabilization (0.1% Triton X-100,20 min). EdU solution was added, the nuclei were stained (Hoechst) and the cells evaluated under fluorescence microscopy.

Measurement of apoptosis

Transfected cells (HT-29 and SW620 cells, pcDNA4.0 vector, pcDNA4.0-PGM1 vector, NC-shRNA, or PGM1-shRNA) were harvested when 90% confluent, stained for 10-15 min with 10 μL Annexin V-APC/7-

AAD apoptosis kit (Lianke Biotech co., LTD., Hangzhou, China) in the dark at room temperatures and evaluated by flow cytometry (FACSCalibur, BD Biosciences, USA).

TUNEL assay

After washing (2x PBS) and fixing (4% paraformaldehyde), cells were stained and visualized using a one-step TUNEL kit (C1089, Beyotime Institute) as previously described [19]. The density of fluorescence was analyzed with Image Pro plus 6.0. CRC tumor tissue sections were dewaxed, incubated with proteinase K (DNase-free, 20 μg/mL, 30 min, 37°C), washed and incubated with 50 μL TUNEL reagents (60 min, 37°C, in the dark). After re-washing in PBS, the sections were evaluated under a confocal fluorescence microscopy (Zeiss LSM710, Germany). Ten randomly selected fields from six sections were used for assessment of apoptotic cells using Image J.

Transwell assays

A 24-well Transwell chamber (8-μm pore size, Corning, NY, USA) was used with or without Matrigel. Transfected cells (5×10^4 in 300 μl serum-free medium) were inoculated in the upper chamber. Medium with 10% FBS (700 μl) was added to the lower chamber, and incubated for 24 h at 37°C. Cells in the lower chamber were fixed (4% paraformaldehyde), stained (0.5% crystal violet), and five randomly selected fields counted and photographed under inverted light microscopy (magnification 200x).

Cell cycle analysis

We analyzed the cell cycle to determine whether PGM1 was involved in its regulation. Briefly, cells were transfected with pcDNA4.0 vector, pcDNA4.0-PGM1 vector, NC-shRNA, or PGM1-shRNA. After harvesting, triplicate samples of cells were fixed (70% ethanol, overnight, 4°C), stained (PI, 100 μg/mL RNAase), and assessed by flow cytometry.

Lactate measurement

Cells (2×10^5) were grown in 12-well plates with a medium change after 10 h. After further incubation for 20 h, lactate was assayed with the Lactate Assay Kit (BioVision, USA). The cells' glycogen levels were measured using the Glycogen Assay Kit (BioVision). Absorbances at 450 nm were read in a microplate reader and lactate concentrations (expressed as means ± SD for three independent samples) were calculated from the standard curve.

ATP measurement

ATP levels were assessed using the ATP Colorimetric/Fluorometric Assay kit (BioVision) following the provided protocol. The phosphorylated glycerol was quantitated by measuring absorbance at 570 nm.

Xenograft mice

Athymic BABL/c nude mice (four weeks old, male) were purchased from the SLAC Laboratory Animal Co. (Shanghai, China). All protocols were approved by the Institutional Animal Care and Use Committee of Wuhan University Zhongnan Hospital. The mice were housed in a pathogen-free location and were randomly assigned to five groups of five animals per group. SW620 cells (3×10^7), either wild-type or transfected with pcDNA4.0 vector, pcDNA4.0-PGM1 vector, NC-shRNA, and PGM1-shRNA) were injected into the left flank. Tumor volumes (calculated from caliper measurements with the formula $V = length \times width^2 \times 0.5$) were determined every third day for four weeks. The mice were then sacrificed and the tumors were fixed (4% paraformaldehyde, 24 h) and stained (H&E) as well as for PGM1 and ki76 using the following antibodies: PGM1 (abcam, #51248: 1:500) and Ki67 (CST, #9449, 1:400). Images were recorded under brightfield microscopy (Olympus, Tokyo, Japan).

Statistical analysis

GraphPad Prism 7.0 (GraphPad, San Diego, CA, USA) was used for data analysis. Data were represented by mean ± standard deviation (SD). The t-test was used for assessing differences between two groups and one-way analysis of variance (ANOVA) for multiple groups. The chi-square test was used for determining the relationship between PGM1 and CRC clinical features. The cut-off value used for patient division into high and low expression groups was the average PGM1 expression value. Survival curves were evaluated by the Kaplan–Meier method and differences were measured by the log-rank test. The Cox proportional hazards model was utilized to determinate independent prognostic factors. $P < 0.05$ was considered statistically significant.

Results

Identification of PGM1 via TCGA datasets

We initially identified differentially expressed genes (DEGs) using the TCGA-CRC data sets. We found that 5463 DEGs, 2524 (12.7%) of which were upregulated, whilst 2939 (14.8%) were downregulated (Fig. 1A). The heatmap shows the top 54 genes that changed the most, in other words, the up- or downregulated genes that were used for further analysis (Fig. 1B). GEPIA is an online resource that allows visualization of TCGA and GTEx data [20]. It can be seen that there was high expression of PGM1 in 41 normal tissues in comparison with 287 colorectal tumor tissues ($P < 0.0001$) (Fig. 1C).

DAVID was used to determine DEG characteristics. GO analysis showed that DEG biological processes (BP) were significantly enriched in "cellular metal ion homeostasis", "muscle system process", and "divalent inorganic cation homeostasis". DEG cell components (CC) were largely enriched in "extracellular matrix" and "collagen-containing extracellular matrix", while molecular function (MF) analysis showed enrichment in "cation transmembrane activity" and "receptor regulator activity" (Fig. 1D). KEGG pathway determination showed DEG enrichment in "neuroactive ligand-receptor interaction", "calcium signaling pathway", and" cytokine-cytokine receptor interaction" (Fig. 1E). Cytoscape was used for drawing the DEG PPI network and identifying significant modules (Fig. 1F).

Furthermore, follow-up data of enrolled patients were collected for survival analysis. Kaplan-Meier curve indicated a worse overall survival in CRC patients with high-level PGM1 (Fig. 1G). ROC curves illustrated the diagnostic potential of PGM1 in CRC with a relatively high sensitivity (AUC=0.635, Fig. 1H). The aforementioned data illustrated that PGM1 could be a prognostic marker for CRC.

Decreased PGM1 in CRC is linked to poor prognosis

To determine the value of the PGM1 level as a CRC biomarker, we used 76 pairs of tumor and matched adjoining normal tissue for measuring PGM1 mRNA levels by RT-PCR. It was observed that CRC expression of PGM1 mRNA was reduced compared to that in the non-CRC tissue ($P<0.001$; Fig. 2A), which was also identified by WB assay (Fig. 2B,C). As verification, IHC was used to evaluate PGM1 protein levels in 100 CRC tissues (Fig. 2D), and the IOD for expression of 100 tumor and normal samples was analyzed by GraphPad Prism. As seen in Fig. 2E, there was lower expression of PGM1 in tumor tissue ($P<0.001$). Moreover, the high-PGM1 patient group yielded a better overall survival rate (P <0.0001; Fig. S2) compared to the low-PGM1 group. These results indicate that PGM1 expression is reduced in CRC tumors and PGM1 expression can affect the survival prognosis in CRC patients.

We also assessed the link between PGM1 levels and clinical characteristics of 76 CRC patients. The ROC curves showed that the best cut-of value of PGM1 expression with optimal discriminatory power was 1.34. On this basis, the 76 immunostained samples were divided into high (index>1.34, n=38) and low (index≤1.34, n=38) expression groups. Table 1 shows a significant relationship between low PGM1 expression and "tumor size" ($P=0.0214$), "lymph node metastasis" ($P=0.00271$), "clinical stage" ($P<0.001$), and "distant metastasis" ($P=0.0365$). However, there was no significant association between PGM1 expression and "age", "sex", or "degree of tumor differentiation". Furthermore, multivariate analysis indicated that "lymphatic node metastasis", "TNM stage", and "distant metastasis" were independent risk factors for poor outcome in CRC patients (Table 2). Consistent with the results in Fig. 1h, Kaplan-Meier analysis indicated a link between lower PGM1 expression and poorer overall survival (OS). Taken together, we deduce that CRC levels of PGM1 are reduced and are linked to poor prognosis.

PGM1-vverexpressing and PGM1-knockdown CRC cell lines were successfully constructed.

To investigate PGM1's role and identify to select the best cell lines for overexpressing or silencing PGM1, PGM1 expression was examined in five lines as well as HCoEpiC cells. Both RT-PCR and Western blotting showed the highest expression in in HT-29 cells ($P<0.001$) and lowest in SW620 cells ($P<0.0001$; Fig. 3A). Silencing by shRNA-1 was most effective in the negative control group (shCTRL, $P<0.001$) (Fig. 3B). Thus, the HT-29 and the SW620 cell lines were selected for silencing PGM1 using shRNA-1. In addition, we also established the CRC cells (SW620 and HT-29) with lentivirus-mediated PGM1 overexpression, which was verified by both qRT-PCR and blotting (Fig. 3C, D, E). Moreover, immunofluorescence confirmed the above experimental results as well (Fig. 3F). These results all demonstrate significant suppression of both protein and mRNA PGM1 levels in sh-PRC1-transfected cells and overexpression in the pcDNA4.0-PGM1 vector transfected cell lines.

Knockdown of PGM1 promotes the proliferation and arrests more cells in S phase

CCK8, colony-forming, and Edu assays were utilized to investigate the effects of PGM1 on proliferation. There was significant inhibition of proliferation in the PGM1 overexpression group in comparison to the negative control group (OE-NC) ($P<0.001$) (Fig. 4A). Similarly, PGM1-Knockdown cells proliferated faster compared with shCTRL group ($P<0.001$). There were (Fig. 4B) diminished colony numbers in the cells transfected with PGM1 overexpression vector (pcDNA4.0-PGM1) (P<0.01) (Fig. 4B), while the opposite phenomenon was seen in the shPGM1 group (shPGM1) in comparison with the shCTRL group. Moreover, the EDU assay also showed reduced cell growth in PGM1 overexpression but enhanced growth with PGM1 knockdown (Fig. 4C).

The distribution of cells in the different groups (CTRL, OE-NC, OE-PGM1, shCTRL, and shPGM1) in the cell cycle was examined with PI. PGM1 silencing resulted in a significant accumulation of S-phase cells and a reduction of cells in G0/G1, while G2/M remained largely unchanged (Fig. 4D) while PGM1 overexpression led to reduced S phase and increased G1 phase. These results suggest that PGM1 exerts tumor suppression by regulating proliferation and enhancing S-phase numbers.

PGM1 promotes apoptosis in CRC cells

Apoptosis is important in CRC. To investigate whether PGM1 acts as a cancer suppressor by modulating apoptosis, we evaluated apoptosis via FCM and TUNEL assays. The result of flow cytometry showed that, in contrast to the shCTRL group, there was a reduced rate of apoptosis in the shPGM1 transfected cells while the rate increased in the PGM1 overexpression cells (Fig. 5A, B). In addition, the TUNEL assay showed that apoptosis was enhanced in the OE-PGM1 group in comparison with the OE-NC group (Fig. 5C, D). On the contrary, PGM1 knockdown greatly decreased HT-29 and SW620 cells apoptosis. These data showed PGM1 promoted apoptosis of CRC cells *in vitro.*

PGM1 inhibits migration and invasion

Transwell assays was used to evaluate the invasive and migratory capacities of colorectal cancer cells influenced by PGM1. Consistent with our previous hypothesis, we found that PGM1 up-regulation markedly reduced the cells' invasion (Fig. 6A, B) and migration (Fig. 6C, D). On the contrary, PGM1 silencing markedly reduced both parameters (Fig. 6A, B, C, D). These findings further confirmed that PGM1 acts as a tumor-suppressing factor in CRC.

PGM1 suppresses CRC through the PI3K/ AKT pathway

Since we hypothesized that PGM1 might have inhibited CRC cells proliferation by downregulation of PI3K/ AKT signaling, we assessed p-PI3K and p-AKT. The diminished p-PI3K and p-AKT protein levels induced by PGM1 overexpression in PI3K/AKT demonstrated substantial upregulation upon transfection with shPGM1 (Fig. 7A, B). Therefore, we conclude that PGM1 inhibits CRC progression at least up to some extent through activating the PI3K/AKT pathway.

We also assessed apoptosis-related proteins. We observed a positive regulation by PGM1 of Bax and a negative regulation of Bcl-2 ($P < 0.05$) (Fig. 7A, B). Thus, it appears that PGM1 exerts tumor suppression by regulating both apoptosis and the S phase.

In terms of cell cycle-related proteins, we found down-regulation of G1 inhibitors (p21) ($P < 0.0001$) and up-regulation of regulatory proteins (Cyclin D1) in shPGM1-transfected cells ($P < 0.0001$, Fig. 7A, B). In contrast, p21 levels were increased ($P < 0.0001$) and Cyclin D1 levels were decreased in response to PGM1 overexpression.

Knockdown of PGM1 accelerates the growth of tumors via the AMPK/ mTOR pathway

We used a mouse tumor model to investigate the action of PGM1 in vivo. SW620 cells transfected with pcDNA4.0 vector, pcDNA4.0-PGM1 vector, NC-shRNA, or PGM1-shRNA were injected into the mice and PGM1 mRNA expression in 5 groups of tumors formed by the different treated cells were determined by RT-PCR (Fig. 8D). Consistent with the previous results of cell experiments, it was observed that tumors in the knockdown group (shPGM1) were markedly larger than seen in the shCTRL group ($P < 0.0001$), and tumors in the PGM1 overexpression group (OE-PGM1) were reduced compared to the control (OE-NC, $P < 0.001$) as shown in Fig. 8A, B, C. Immunohistochemical analysis of the tumor tissues indicated reduced expression of the differentiation marker Ki67 ($P < 0.05$, Fig. 8E). Moreover, the TUNEL assay showed that PGM1 overexpression (OE-PGM1) led to more apoptosis than in the control (OE-NC), although apoptosis was reduced in the PGM1 knockdown group (shPGM1), in comparison with the shCTRL group (Fig. 8E). Thus, PGM1 inhibition leads to a suppression of CRC growth and enhances differentiation. Western blotting was used to examine changes in p-PI3K and p-AKT expression. This is consistent with the aforementioned cell experiment (Fig. S1). Therefore, we further confirmed that PGM1 inhibits CRC progression via activation of the AMPK/ mTOR pathway.

PGM1 knockdown enhances glycolysis to promote proliferation

PGM1 assists in regulating the balance between glycogen synthesis and glycolysis by reversibly catalyzing phosphate transfer in glucose. Because of this, we investigated whether this might affect PGM1's role in suppressing tumor growth. It was found that PGM1 overexpression inhibited both lactate and ATP in HT-29 cells while knockdown increased the production of both (Fig. 9A, B). This was confirmed in SW620 cells (Fig. 9A, B). These findings indicated that PGM1 regulates the aerobic glycolysis process of CRC cells.

Discussion

There are five proteins in the PGM superfamily: PGM1, PGM2, PGM2L1, PGM3, and PGM5. Despite their structural similarities, the substrates and functions of these proteins differ [9, 21, 22]. PGM3, for example, is an N-acetylglucosamine triphosphatase that participate in alanine biosynthesis and has anti-neoplastic functions. Targeting PGM3 inhibits the hexosamine synthetic pathway and has been found to result in growth arrest and apoptosis in breast cancer [23], and blocking PGM3 expression by sulforaphane

promotes apoptosis in prostate cancer cells [24]. PGM5 is strongly expressed in muscle connections [25], and its expression level is predictive of overall survival in CRC [10]. PGM1's function in glucose homeostasis and posttranslational glycosylation is well characterized, and the enzyme plays an important role in glucose trafficking through catalysis of the G1-P to G6-P conversion. PGM1 deficiency is recognized as an inherited metabolic disorder (CDG1T) [21] associated with a variety of phenotypes including exercise intolerance, dilated cardiomyopathy, and liver disease, indicative of the role of the enzyme in glucose metabolism [26]. However, PGM1's role in cancer is poorly understood.

Studies on the PGM1 in cancer are limited. Recent studies have shown that PGM1 blocks liver cancer progression through regulation of glucose trafficking [15]. Nevertheless, a high expression of PGM1 was noted in lung tumors, correlating poor prognosis. Li et al. [16] suggested that activation of AMPK following glucose deprivation results in increased PGM1 expression that enhances cancer progression, suggesting the possibility of targeting PGM1. Thus, PGM1 does not show consistent expression patterns in different cancer types, possibly related to the content of muscle.

Metastasis involves factors related to both the tumor and its microenvironment [27]. The microenvironment is comprised of neighboring tumor cells, extracellular matrix, and interstitial tissue [28–30]. The rapid proliferation shown by tumors requires a significant amount of resources, and tumors are characterized by alterations in their metabolism [31] involving reconstruction of energy metabolism [32].

PGM1, thus, is vital for glucose metabolism and its absence leads to deficiencies in glycogen metabolism that, in turn, result in disease [33–35]. Specifically, PGM1 encodes a phosphoglucomutase associated with carbohydrate metabolism [7]. Therefore, we proposed that reduced levels of PGM1 adversely affect energy metabolism, leading to a remodeling of tumor cell physiology with a shift to the use of aerobic glycolysis. We also demonstrated that reduced PGM1 in CRC cells stimulates both cellular proliferation and tumor growth through a shift from glycogen synthesis to divert glucose to the glycolytic pathways. Our results point to PGM1 having a unique, glucose-dependent role in the suppression of CRC tumors. Recently, it was found that PGM1's role in glycogen and glucose metabolism is responsible for suppressing proliferation in cervical and breast cancer cells [36]. Our findings support this. All these results suggest that PGM1 may promote or inhibit tumor formation dependent on the tissue context.

PI3K/Akt signaling promotes proliferation and cell survival, and is associated with neoplastic transformation and apoptosis inhibition [37]. It is also known that there is aberrant expression of the proteins of the pathway and that this is linked to the progression of a variety of cancers [38–40]. Apart from proliferation, the pathway is also linked to migration and autophagy [41, 42]. Therefore, research on PGM1 and whether it targets the PI3K/AKT pathway may be significant for the management of CRC. Here, we demonstrate that PI3K/AKT is closely linked to PGM1 expression regulation to maintain cancer cell survival and proliferation. This association is important in advancing our understanding of in devising new therapeutic strategies, indicating that the targeting of glycogen metabolism may have

potential for developing treatments for a variety of cancers that show aberrations in these pathways as well as PGM1 expression.

Taken together, these findings show that PGM1 suppresses CRC by regulating glucose translocation via the PI3K/ AKT pathway and that PGM1 may be a potential target for treating and predicting the course of therapeutic and predictive target for CRC.

Conclusion

We have shown that PGM1 suppresses CRC and is significantly downregulated in CRC. In addition, lower levels of PGM1 were associated with poor prognosis. On the other hand, PGM1 overexpression reduced proliferation, invasion, and migration in CRC cells. PGM1 may thus be a new biomarker and treatment target for CRC.

Abbreviations

PGM: phosphoglucomutase

CRC: colorectal cancer

TCGA: The Cancer Genome Atlas

DEG: differentially expressed genes

TMA: tissue microarray

Declarations

Authors' contributions

Conception and design: YFZ. Development of Methodology: ZWZ, XZ, JB. Acquisition of data: ZWZ, XZ, JB, LL , DL. Analysis and interpretation of data: LL, DL. Writing, review, and/or revision of the manuscript: YFZ, XZ, ZWZ wrote the initial draft and all authors reviewed the manuscript. Study Supervision: YFZ and ZWZ. All authors read and approved the final manuscript.

Acknowledgements

We thank all those who participated in this study.

Availability of data and materials

The datasets used in this study are available from the corresponding author upon reasonable request.

Ethics approval and consent to participate

We were used for patients tissues experiments with the ethical approval of Wuhan University Zhongnan Hospital.

Consent for publication

Authors involved in this paper all signed written consent for publishing in your journal.

Competing interests

The authors declare no conflicts of interest.

Contributor Information

Zhewen Zheng, Email: 2018163030003@whu.edu.cn.

Xue Zhang, Email: Vowwzx@163.com.

Jian Bai, Email: xybaijian@163.com.

Long Long, Email: longlong1125@whu.edu.cn.

Di Liu, Email: 954184267@qq.com.

Yunfeng Zhou, Email: yfzhouwhu@163.com, 2017103030046@whu.edu.cn.

References

1. Brody H. Colorectal cancer. Nature. 2015,521:S1. doi: 10.1038/521S1a.
2. Siegel RL, Miller KD, Jemal A. Cancer statistics, 2020. CA Cancer J Clin. 2020,70:7-30. doi: 10.3322/caac.21590.
3. Modest DP, Pant S, Sartore-Bianchi A. Treatment sequencing in metastatic colorectal cancer. Eur J Cancer. 2019,109:70-83. doi: 10.1016/j.ejca.201 8.12.019.
4. Ladabaum U, Dominitz JA, Kahi C, Schoen RE. Strategies for Colorectal Cancer Screening. Gastroenterology. 2020,158:418-432. doi: 10.1053/j.gas tro.2019.06.043..
5. Zaka Abbaszadeh, Selin Çeşmeli, Çığır Biray Avcı. Crucial players in glycolysis: Cancer progress. Gene. 2020,726:144158. doi: 10.1016/j.gene.201 9.144158.
6. Zhang X, Zhao H, Li Y, Xia D, Yang L, Ma Y, Li H. The role of YAP/TAZ activity in cancer metabolic reprogramming. Mol Cancer. 2018,17:134. doi: 10.1186/s12943-018-0882-1.

7. Ashton TM, McKenna WG, Kunz-Schughart LA, Higgins GS. Oxidative Phosphorylation as an Emerging Target in Cancer Therapy. Clin Cancer Res. 2018,24:2482-2490. doi: 10.1158/1078-04 32.CCR-17-3070.

8. Koppenol WH, Bounds PL, Dang CV. Otto Warburg's contributions to current concepts of cancer metabolism. Nat Rev Cancer. 2011,11:325-37. doi: 10.1007/s00109-011-0730-x.

9. Muenks AG, Stiers KM, Beamer LJ. Sequence-structure relationships, expression profiles, and disease-associated mutations in the paralogs of phosphoglucomutase 1. PLoS One. 2017,12:e0183563.

10. Yifan Sun, Haihua Long, Lin Sun, Xiujuan Sun, Liping Pang, Jianlin Chen, et al. PGM5 is a promising biomarker and may predict the prognosis of colorectal cancer patients. Cancer Cell Int. 2019,19:253. doi: 10.1186/s12935-019-0967-y.

11. Marion Curtis, Hilary A Kenny, Bradley Ashcroft, Abir Mukherjee, Alyssa Johnson, Yilin Zhang, et al. Fibroblasts Mobilize Tumor Cell Glycogen to Promote Proliferation and Metastasis. Cell Metab. 2019,29:141-155.e9. doi: 10.1016/j.cmet.2018.08.007.

12. Federica Conte, Eva Morava, Nurulamin Abu Bakar, Saskia B Wortmann, Anne Jonge Poerink, Stephanie Grunewald, et al. Phosphoglucomutase-1 deficiency: Early presentation, metabolic management and detection in neonatal blood spots. Mol Genet Metab. 2020,131:135-146. doi: 10.1016/j.ymgme.2020.08.003.

13. Yanping Li, Ronghui Liang, Mingming Sun, Zhen Li, Hao Sheng, Jiyan Wang, et al. AMPK-dependent phosphorylation of HDAC8 triggers PGM1 expression to promote lung cancer cell survival under glucose starvation. Cancer Lett. 2020,478:82-92. doi: 10.1016/j.canlet.2020.03.007.

14. K J Livak, T D Schmittgen. Analysis of relative gene expression data using real-time quantitative PCR and the 2(-Delta Delta C(T)) Method. Methods. 2001,25:402-408. doi: 10.1006/meth.2001.1262.

15. Im K, Mareninov S, Diaz MFP, Yong WH. An Introduction to Performing Immunofluorescence Staining. Methods Mol Biol. 2019,1897:299-311. doi: 10.1007/978-1-4939-8935-5_26.

16. Xiao-Wan Wang, Rui-Min Tian, Yi-Qi Yang, Zhao-Yu Lu, Xiao-Dong Han, Xu-Sheng Liu, et al. Triptriolide antagonizes triptolide-induced nephrocyte apoptosis via inhibiting oxidative stress in vitro and in vivo. Biomed Pharmacother. 2019,118:109232. doi: 10.1016/j.biopha.2019.109232.

17. Tang Z, Li C, Kang B, Gao G, Li C, Zhang Z. GEPIA: a web server for cancer and normal gene expression profiling and interactive analyses. Nucleic Acids Res. 2017,45:W98-W102. doi: 10.1093/nar/gkx247.

18. Ruqaiah Altassan, Silvia Radenkovic, Andrew C Edmondson, Rita Barone, Sandra Brasil, Anna Cechova, et al. International consensus guidelines for phosphoglucomutase 1 deficiency (PGM1-CDG): Diagnosis, follow-up, and management. J Inherit Metab Dis. 2021,44:148-163. doi: 10.1002/jimd.12286.

19. Jing-Jing Liu, Guo-Chang Zhang, In Iok Kong, Eun Ju Yun, Jia-Qi Zheng, Dae-Hyuk Kweon, et al. A Mutation in PGM2 Causing Inefficient Galactose Metabolism in the Probiotic Yeast Saccharomyces boulardii. Appl Environ Microbiol. 2018,84:e02858-17. doi: 10.1128/AEM.02858-17.

20. Francesca Ricciardiello, Giuseppina Votta, Roberta Palorini, Isabella Raccagni, Laura Brunelli, Alice Paiotta, et al. Inhibition of the Hexosamine Biosynthetic Pathway by targeting PGM3 causes breast cancer growth arrest and apoptosis. Cell Death Dis. 2018,9:377. doi: 10.1038/s41419-018-0 405-4.

21. Chan-Hee Lee, Soo-Jin Jeong, Sun-Mi Yun, Ji-Hyun Kim, Hyo-Jung Lee, Kwang Seok Ahn, et al. Down-regulation of phosphoglucomutase 3 mediates sulforaphane-induced cell death in LNCaP prostate cancer cells. Proteome Sci. 2010,8:67. doi: 10.1186/1477-5956-8-67.

22. Belkin AM, Klimanskaya IV, Lukashev ME, Lilley K, Critchley DR, Koteliansky VE. A novel phosphoglucomutase-related protein is concentrated in adherens junctions of muscle and nonmuscle cells. J Cell Sci. 1994,107:159-173.

23. Wo-Tu Tian, Xing-Hua Luan, Hai-Yan Zhou, Chao Zhang, Xiao-Jun Huang, Xiao-Li Liu, et al. Congenital disorder of glycosylation type 1T with a novel truncated homozygous mutation in PGM1 gene and literature review. Neuromuscul Disord. 2019,29:282-289. doi: 10.1016/j.nmd.2019.01.001.

24. Laplane L, Duluc D, Bikfalvi A, Larmonier N, Pradeu T. Beyond the tumour microenvironment. Int J Cancer. 2019,145:2611-2618. doi: 10.1002/ijc.32343.

25. Arneth B.Tumor Microenvironment. Medicina (Kaunas). 2019,56:15. doi: 10.3390/medicina560 10015.

26. Sandra S McAllister, Robert A Weinberg. The tumour-induced systemic environment as a critical regulator of cancer progression and metastasis. Nat Cell Biol. 2014,16:717-727. doi: 10.1038/ncb3015.

27. Wu T, Dai Y. Tumor microenvironment and therapeutic response. Cancer Lett. 2017,387:61-68. doi: 10.1016/j.canlet.2016.01.043.

28. Biswas SK. Metabolic R Guang-Zhi Jin, Yajuan Zhang, Wen-Ming Cong, Xueyuan Wu, Xiongjun Wang, Siyang Wu, et al. Phosphoglucomutase 1 inhibits hepatocellular carcinoma progression by regulating glucose trafficking. PLoS Biol. 2018,16:e2006483. doi: 10.1371/journal.pbio.2006483. eprogramming of Immune Cells in Cancer Progression. Immunity. 2015,43:435-449. doi: 10.1016/j.immuni.2015.09.001.

29. Hanahan D, Weinberg RA. Hallmarks of cancer: the next generation. Cell. 2011,144:646-674. doi: 10.1016/j.cell.2011.02.013.

30. Lesa J Beamer. Enzyme dysfunction at atomic resolution: Disease-associated variants of human. phosphoglucomutase-1. Biochimie. 2021,183:44-48. doi:10.1016/j.biochi.2020. 08.017.

31. Eva Fernlund, Oskar Andersson, Rada Ellegård, Hanna Klang Årstrand, Henrik Green, Hans Olsson, et al. The congenital disorder of glycosylation in PGM1 (PGM1-CDG) can cause severe cardiomyopathy and unexpected sudden cardiac death in childhood. Forensic Sci Int Genet. 2019,43:102111. doi: 10.1016/j.fsigen.20 19.06.012.

32. Guang-Zhi Jin, Yajuan Zhang, Wen-Ming Cong, Xueyuan Wu, Xiongjun Wang, Siyang Wu, et al. Phosphoglucomutase 1 inhibits hepatocellular carcinoma progression by regulating glucose trafficking. PLoS Biol. 2018,16:e2006483. doi: 10.1371/journal.pbio.2006483.

33. Tegtmeyer LC, Rust S, van Scherpenzeel M, Ng BG, Losfeld ME, et al. Multiple phenotypes in phosphoglucomutase 1 deficiency. N Engl J Med. 2014, 370(6):533-542. doi: 10.1056/NEJMoa1206605.

34. Du L, Prabhakaran V, Xie X, Park S, Wang Y, Shao Y. Low-PGM and PGM-Free Catalysts for Proton Exchange Membrane Fuel Cells: Stability Challenges and Material Solutions. Adv Mater. 2021 Feb,33(6):e1908232. doi: 10.1002/adma.201908232.

35. Martinez U, Komini Babu S, Holby EF, Chung HT, Yin X, Zelenay P: **Progress in the Development of Fe-Based PGM-Free Electrocatalysts for the Oxygen Reduction Reaction**. *Adv Mater* 2019, **31**(31):e1806545.

36. Bae E, Kim HE, Koh E, Kim KS. Phosphoglucomutase1 is necessary for sustained cell growth under repetitive glucose depletion. FEBS Lett. 2014, 588(17):3074-80. doi: 10.1016/j.febslet.2014.06.034.

37. Chelh I, Picard B, Hocquette JF, Cassar-Malek I. Myostatin inactivation induces a similar muscle molecular signature in double-muscled cattle as in mice. Animal. 2011, 5(2):278-86. doi: 10.1017/S1751731110001862.

38. Marquard FE, Jücker M. PI3K/AKT/mTOR signaling as a molecular target in head and neck cancer. Biochem Pharmacol. 2020, 172:113729. doi: 10.1016/j.bcp.2019.113729.

39. Alzahrani AS. PI3K/Akt/mTOR inhibitors in cancer: At the bench and bedside. Semin Cancer Biol. 2019,59:125-132. doi: 10.1016/j.semcancer.2019.07.009.

40. Sharma VR, Gupta GK, Sharma AK, Batra N, Sharma DK, Joshi A, Sharma AK. PI3K/Akt/mTOR Intracellular Pathway and Breast Cancer: Factors, Mechanism and Regulation. Curr Pharm Des. 2017,23(11):1633-1638. doi: 10.2174/138161282366616 1116125218.

41. Park JY, Kang SE, Ahn KS, Um JY, Yang WM, Yun M, et al. Inhibition of the PI3K-AKT-mTOR pathway suppresses the adipocyte-mediated proliferation and migration of breast cancer cells. J Cancer. 2020,11(9):2552-2559. doi: 10.7150/jca.37975. PMID: 32201525.

42. Xu Z, Han X, Ou D, Liu T, Li Z, Jiang G, et al. Targeting PI3K/AKT/mTOR-mediated autophagy for tumor therapy. Appl Microbiol Biotechnol. 2020,104(2):575-587. doi: 10.1007/s00253-019-10257-8.

Tables

Table 1. Associations of PGM1 expression with clinicopathological factors in CRC patients

Variable	Number	PGM1 Expression		P-value
		High	Low	
		(N=38)	(N=38)	
Age(year)				
< 65	59 (77.6%)	31 (81.6%)	28 (73.7%)	0.582
≥ 65	17 (22.4%)	7 (18.4%)	10 (26.3%)	
Gender				
Female	32 (42.1%)	12 (31.6%)	20 (52.6%)	0.104
Male	44 (57.9%)	26 (68.4%)	18 (47.4%)	
Tumor size (cm)				
< 5	41 (53.9%)	26 (68.4%)	15 (39.5%)	0.0214
≥ 5	35 (46.1%)	12 (31.6%)	23 (60.5%)	
Differentiation				
Moderate	19 (25.0%)	9 (23.7%)	10 (26.3%)	0.447
Poor	34 (44.7%)	15 (39.5%)	19 (50.0%)	
Well	23 (30.3%)	14 (36.8%)	9 (23.7%)	
Lymphatic node metastasis				
Negative	42 (55.3%)	28 (73.7%)	14 (36.8%)	0.00271
Positive	34 (44.7%)	10 (26.3%)	24 (63.2%)	
TNM stage				
I+II	34 (44.7%)	25 (65.8%)	9 (23.7%)	<0.001
III+IV	42 (55.3%)	13 (34.2%)	29 (76.3%)	
Distant metastasis				
No	44 (57.9%)	27 (71.1%)	17 (44.7%)	0.0365
Yes	32 (42.1%)	11 (28.9%)	21 (55.3%)	

Table 2. Multivariate analysis of the correlation between PGM1 expression and clinicopathologic parameters

| Parameters	B	p	OR	95% CI
Tumor size (cm)⬚≥ 5	-1.114	0.063	0.328	0.101-1.063
Lymphatic node metastasis⬚Positive	-1.605	0.006	0.201	0.064-0.635
TNM stage⬚III + IV	-1.391	0.018	0.249	0.079-0.784
Distant metastasis⬚Yes	-1.215	0.037	0.297	0.095-0.928

Figures
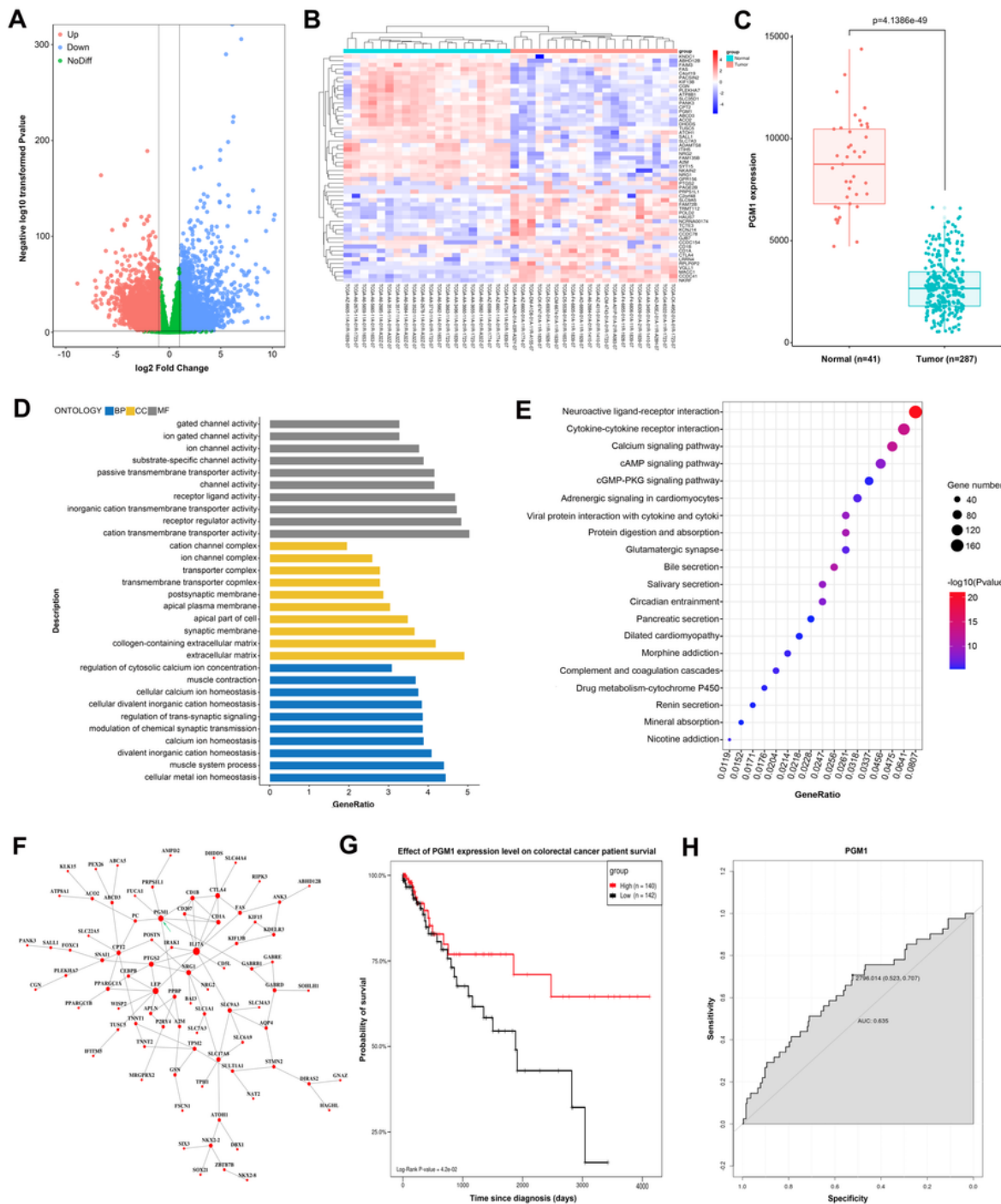
Figure 1

Identification of PGM1 via TCGA datasets. (A) Volcano plot chart showing the distribution of the DEGs in TCGA. Red color shows up-regulated genes while blue color shows down-regulated genes. (B) Heatmap of 54 core genes from the TCGA-COAD dataset comparing CRC and adjoining normal tissue. (C) PGM1 expression in normal controls and CRC patients using samples from the TCGA database (matched TCGA normal and GTEx data, P<0.001). Each dot represents one sample, (D) GO network showing relationships

between DEGs and predicted functions. Vertical axis, GO category, horizontal axis, P-values. Lower P-values indicate greater predicted involvement of DEGs in CRC+. (E) KEGG network showing connections between pathways and DEGs. Vertical axis, pathway classification, horizontal axis, P-value. Lower P-values indicate greater numbers of pathways that involve DEGs. (F) PPI (protein-protein interaction) network of DEGs drawn by Cytoscape. (G) Kaplan–Meier analysis showing association between PGM1 expression and overall survival in CRC patients. (H) AUC curves with respect to the PGM1 gene expression in the TCGA cohort. PGM phosphoglucomutase, CRC colorectal cancer, TCGA The Cancer Genome Atlas, AUC area under the curve.
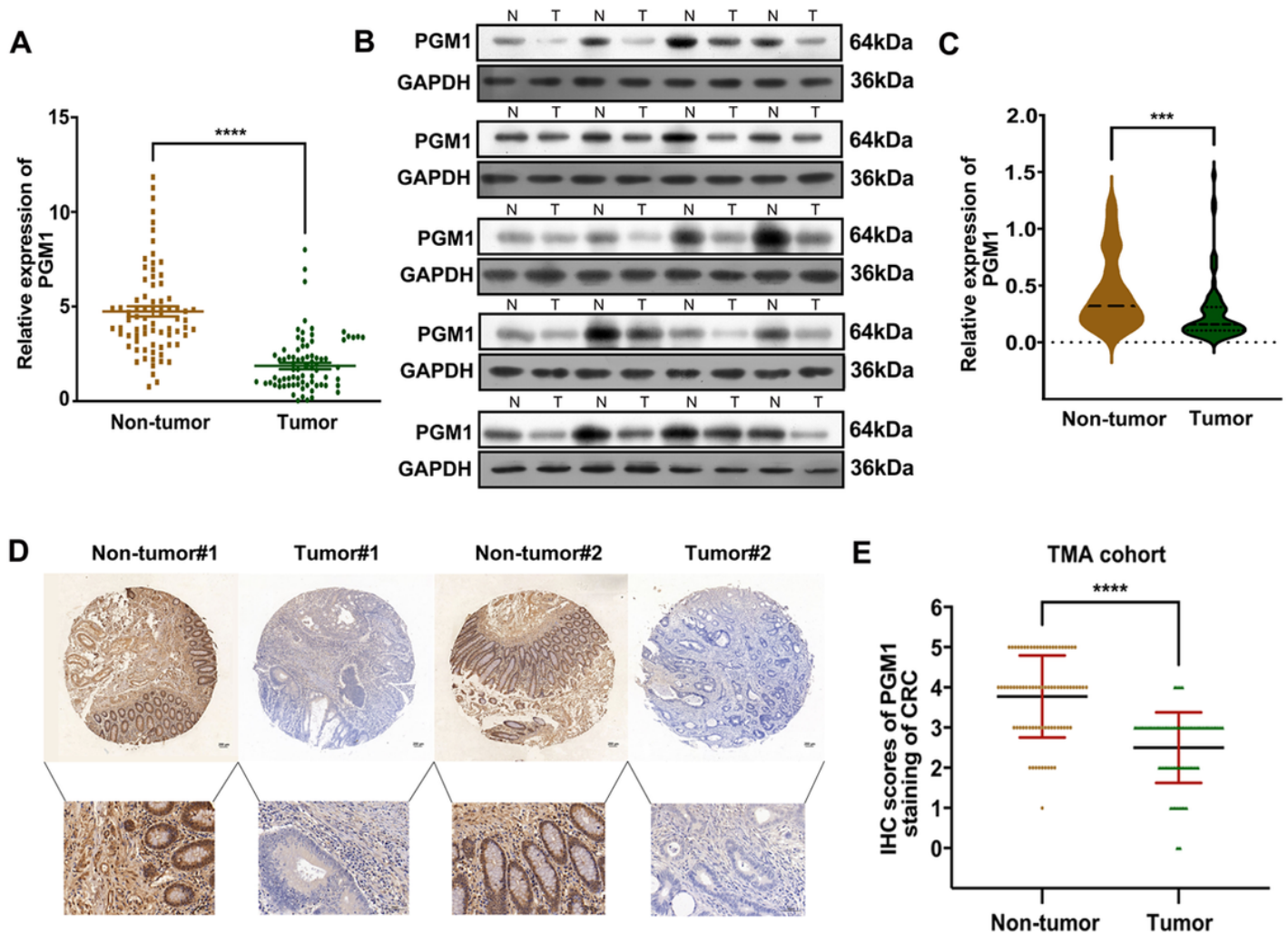
Figure 2

Downregulated PGM1 is linked to poor prognosis. (A) Expression of PGM1 mRNA using RT-PCR in CRC and normal tissues (n=76), (B) PGM1 protein levels in tumor and non-tumor tissues. (C) PGM1 protein levels in paired tumor and non-tumor samples (n=76), (D-E) PGM1 IHC TMA images contained 100 tumor and non-tumor tissue pairs (×200, scale bar 100 μm), respectively. Quantification of cell number is shown. ***<0.001, ****<0.0001.
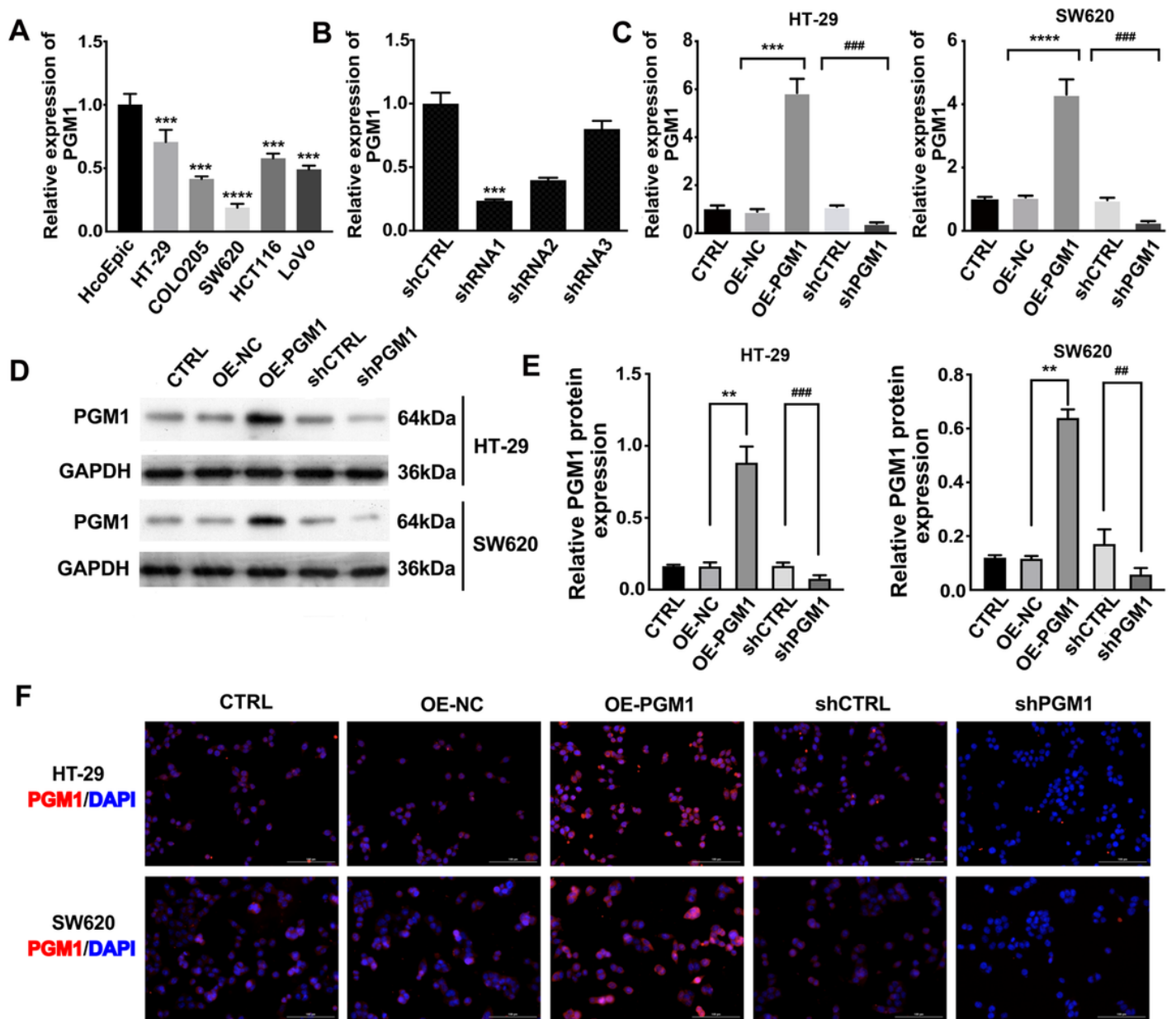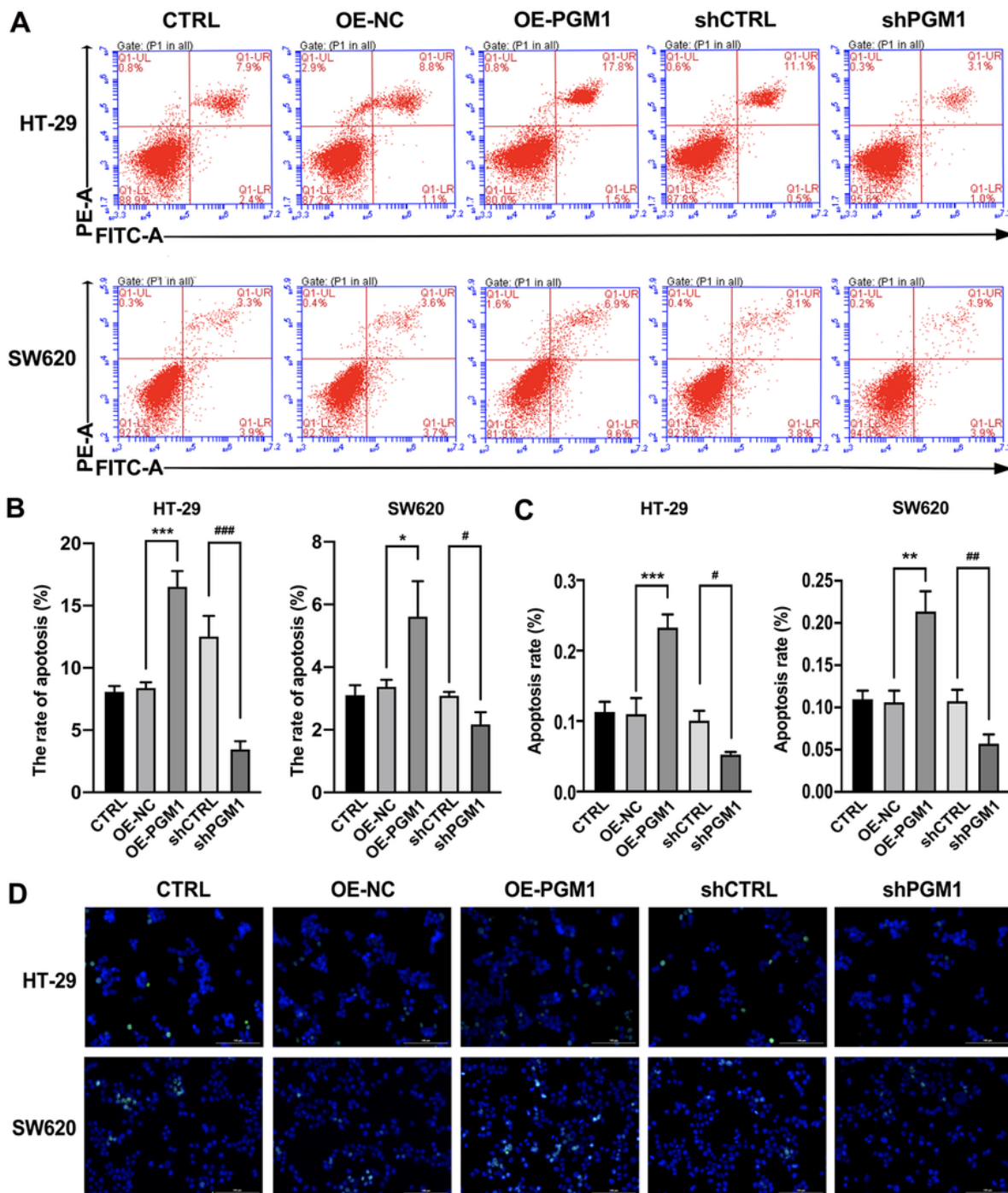
Figure 3

Successful construction of PGM1-overexpression and knockdown lines. (A) The PGM1 expression in CRC cells measured by RT-PCR. (B) PGM1 mRNA in control cells and in cells transfected with PGM1 shRNA. ***P<0.01 vs. shCTRL. (C) PGM1 mRNA expression in cells transfected with pcDNA4.0 vector, pcDNA4.0-PGM1 vector, NC-shRNA, or PGM1-shRNA were determined by RT-qPCR. (D-E) PGM1 protein expression in cells transfected with indicated vectors, which divided into five groups, including CTRL, OE-NC, OE-PGM1, shCTRL and shPGM1. (F) Images of cells transfected with afore mentioned vectors or shRNAs stained for PGM1 (red), nuclei are stained blue (DAPI). IOD integrated optical density, R CTRL negative control, OE over expression. Data are means ± SD from three replicates of each sample, **P<0.01, ***P<0.001, ****P<0.001, ## P<0.01, ### P<0.001.
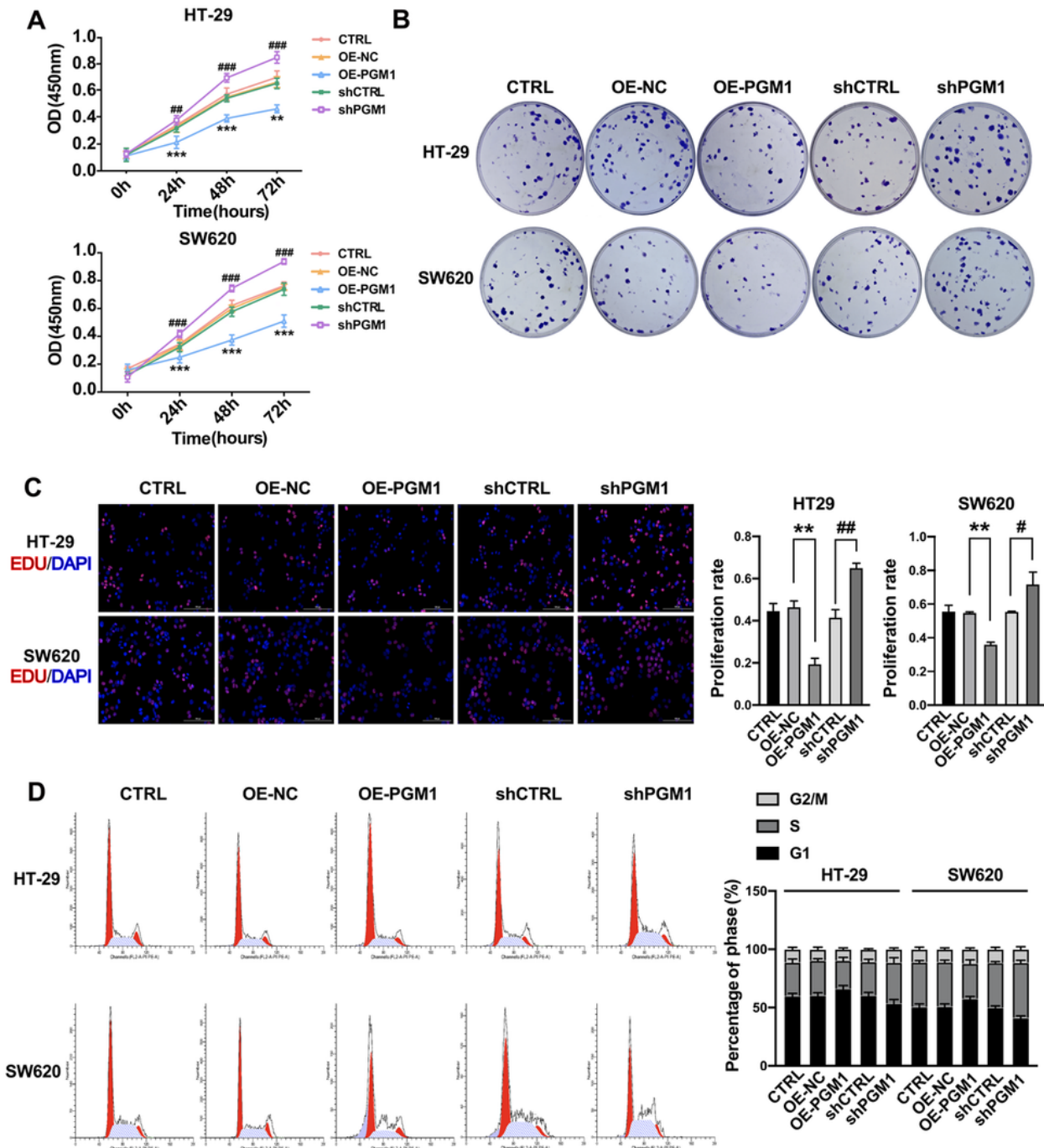
Figure 4

PGM1 knockdown promotes proliferation and arrested more cells in S phase. (A) PGM1 overexpression markedly inhibits proliferation in HT29 and SW620, while knockdown of PGM1 markedly promotes the proliferation in HT29 and SW620. (B) Colony formation capacity of CTRL, OE-NC, OE-PGM1, shCTRL and shPGM1 groups in HT-29 and SW620 cells, (C) EdU assay comparing proliferation in CTRL, OE-NC, OE-PGM1, shCTRL and shPGM1 groups in HT-29 and SW620 cells (scale bar, 100 μm), (D) Flow chart

showing the distribution of the proportions of different cell cycles in the HT-29 or SW620 of the 5 groups, respectively. Data are means ± SD from three replicates of each sample, *P<0.05, **P<0.01, ***P<0.001, ## P<0.01, ### P<0.001, #### P<0.0001.

Figure 5

PGM1 promotes apoptosis. (A-B) The ratio of apoptosis in cells transfected with indicated vectors, which consisting of the CTRL, OE-NC, OE-PGM1, shCTRL and shPGM1 groups were measured using flow

cytometry. Apoptosis ratios in the five groups. Bars indicate mean rate ± SD. (C-D) TUNEL assay of apoptosis in CTRL, OE-NC, OE-PGM1, shCTRL, and shPGM1 groups in HT-29 and SW620 cells (scale bar, 100 μm). HE: hematoxylin-eosin , *P<0.05, **P<0.01, ***P<0.001, #P<0.05, ## P<0.01, ### P<0.001.

Figure 6

PGM1 inhibits invasion and migration. (A) Migration ability in cell lines. (B) Apoptosis rates. (C) Apoptosis measured by TUNEL. (D) TUNEL images. ****P<0.001, #### P<0.0001.
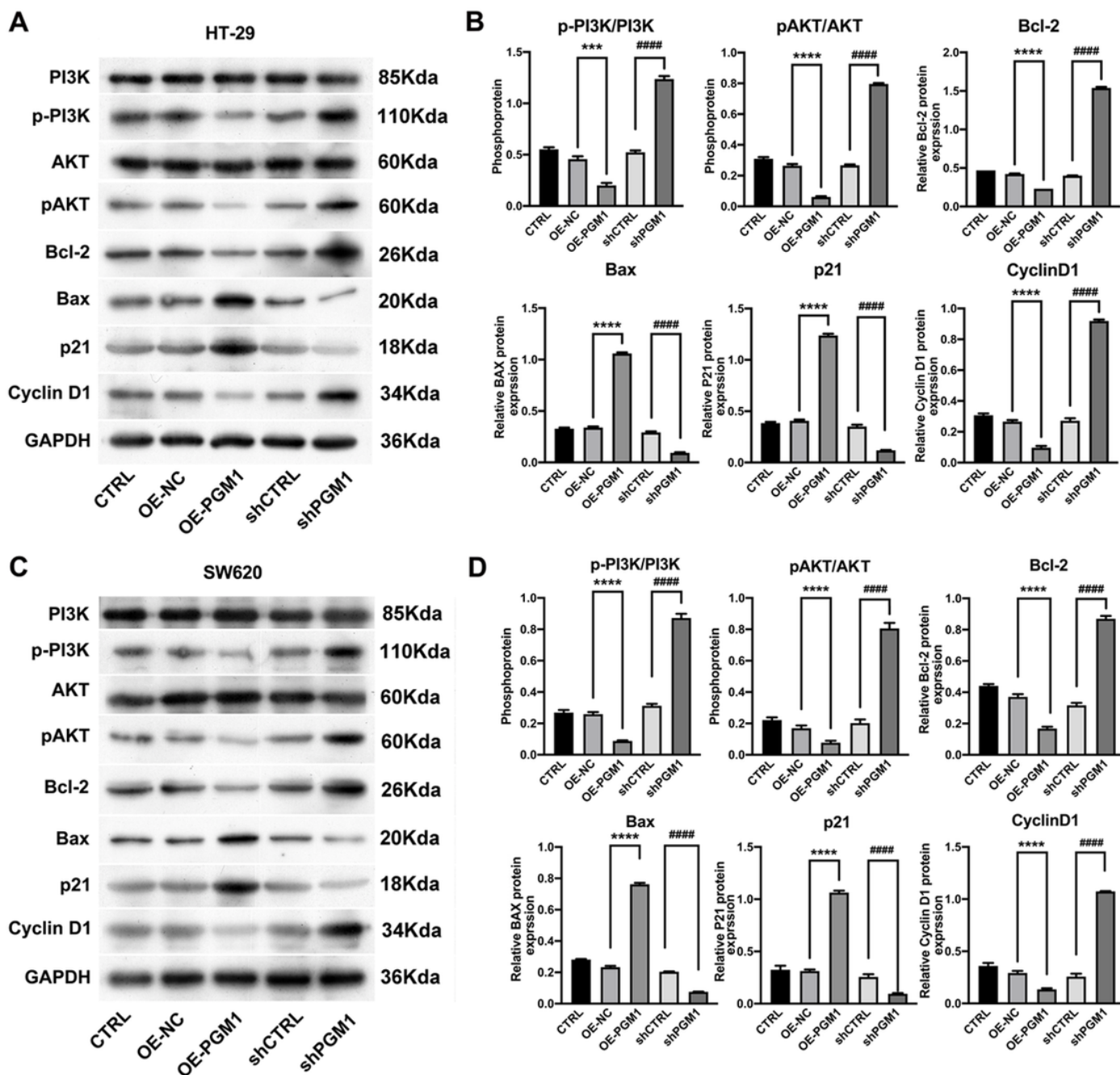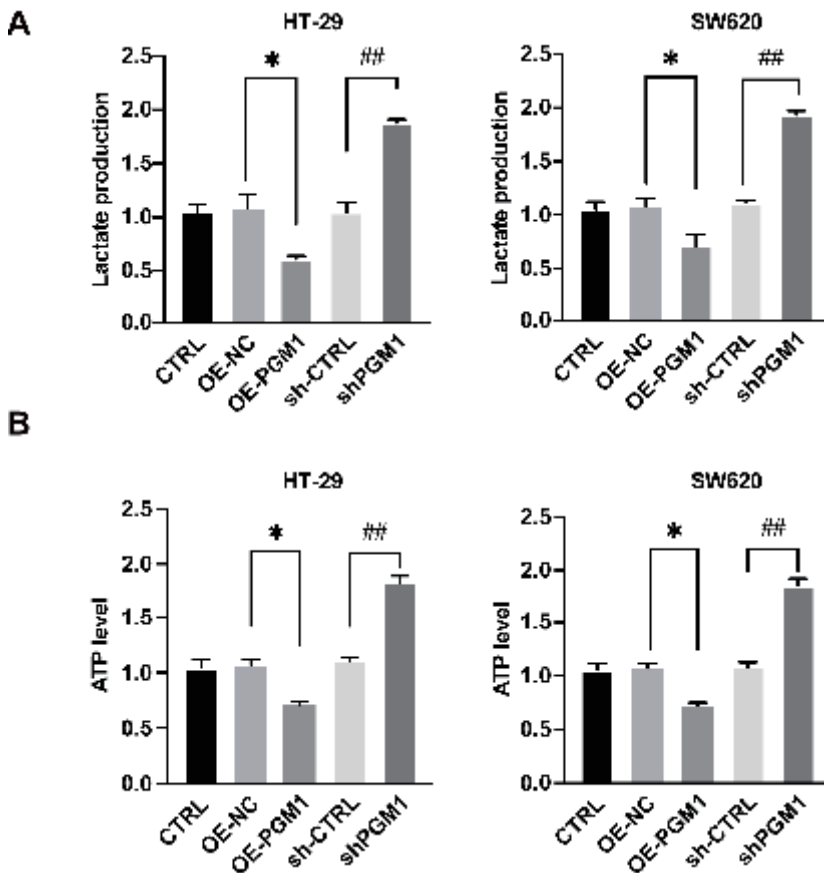

Figure 7

PGM1 action is related to the PI3K/ AKT pathway. (A) Expression level of PI3K, p-PI3K, AKT, p-AKT, Bcl-2, BAX, P21 and Cyclin D1 in the HT-29 cell of the 5 groups (CTRL, OE-NC, OE-PGM1, shCTRL and shPGM1 groups) shown by western blotting. (B) Protein expression shown by densitometry. Data were normalized to GAPDH and were from three experiments. (C) Expression levels of PI3K, p-PI3K, AKT, p-AKT, Bcl-2, BAX, P21 and Cyclin D1 in SW620 cells of the 5 groups (CTRL, OE-NC, OE-PGM1, shCTRL, and shPGM1) shown by western blotting. (D) Protein expression shown by densitometry. Data were normalized to GAPDH and were from three separate experiments. ***P<0.001, ****P<0.0001, ####P<0.0001.

Figure 8

Downregulation of PGM1 accelerates tumor growth in vivo. (A) Tumors formed 6 weeks post-injection. Tumors in the CTRL, OE-NC, OE-PGM1, shCTRL and shPGM1 groups were removed on completion of the study. (B) Growth of tumors was assessed by tumor volume measurement over time in the 5 groups (mean ± SD, n=25). **P<0.01. Mice were anesthetized and sacrificed at experimental endpoints. Tumors were subsequently dissected. (C) Tumor volume was monitored in the 5 afore mentioned groups at the endpoint of experiments. (D) PGM1 mRNA expression in tumors from CTRL, OE-NC, OE-PGM1, shCTRL and shPGM1 groups, n = 5. (E) Representative images of PGM1 IHC, HE, Ki67 and TUNEL staining in CTRL, OE-NC, OE-PGM1, shCTRL and shPGM1 groups, respectively. (×200, scale bars, 100 μm). **P<0.01, ***P<0.001, ###P<0.001, ####P<0.0001.

Figure 9

PGM1 inhibits aerobic glycolysis in CRC. (A–B) Cells were transfected with lentivirus expressing CTRL, OE-NC, OE-PGM1, shCTRL, or shPGM1. Culture media were used for determining lactate production (panel A) and ATP level (panel B) of these cells were measured. Data are means ± SD of 3 independent experiments. *P<0.05, ##P<0.01.

Supplementary Files

This is a list of supplementary files associated with this preprint. Click to download.

- FigureS1.png
- FigureS2.png
- TableS1.doc